NUKLEONIKA 2011;56(2):85–98

ORIGINAL PAPER

Generation and diagnostics of fast electrons within tokamak plasmas

Marek J. Sadowski

Abstract. The first part of this invited paper is devoted to mechanisms of the production of fast electrons in plasma experiments involving magnetic traps of the tokamak type. The phenomenon of generation of the so-called runaway electrons – which may reach energies up to several dozen MeV – is considered and basic characteristics of such electrons are described. In particular, the orbits of the runaway electrons and their energy limits are presented. Problems related to the cross-field transport in tokamak plasmas and interactions of the relativistic electrons with plasma oscillations are also considered. Production of the so-called ripple-born electrons, which may be observed in the energy range from approximately 50 keV to several hundreds keV, is analyzed separately. In the second part of this paper various diagnostic methods used for investigation of the runaway and ripple-born electrons are presented. Various techniques are described, which are based on different reactions induced by the runaway electrons, e.g., the emission of X-rays or neutrons, or the synchrotron radiation. Finally, a modern technique of electron measurements is described, which was developed by the author's team at the Andrzej Sołtan Institute for Nuclear Studies (IPJ) in Świerk (Poland), and which is based on the use of Cherenkov-type detectors. Examples of applications of the discussed techniques in different tokamak experiments are described. Particular attention is paid to the Cherenkov detectors, which have already been used in experiments at the small-size CASTOR device in Prague (Czech Republic), the ISTTOK machine in Lisbon (Portugal), as well as in the larger TORE-SUPRA facility in Cadarache (France).

Key words: tokamak • runaway electrons • ripple-born electrons • Cherenkov detectors

M. J. Sadowski
The Andrzej Soltan Institute for Nuclear Studies (IPJ),
05-400 Otwock/Świerk, Poland
and Institute of Plasma Physics and Laser Microfusion (IPPLM),
23 Hery Str., 01-497 Warsaw, Poland,
Tel.: +48 22 718 0537, Fax: +48 22 779 3481,
E-mail: msadowski@ipj.gov.pl

Received: 22 June 2010
Accepted: 30 August 2010

Introduction

The initial generation, heating and confinement of plasma in toroidal magnetic traps of the tokamak type is achieved by driving a current through a ring-shaped vacuum chamber, which is filled with a gas (usually deuterium) under a low pressure. This current is generated by an induced electric field produced in the toroidal direction, as shown in Fig. 1.

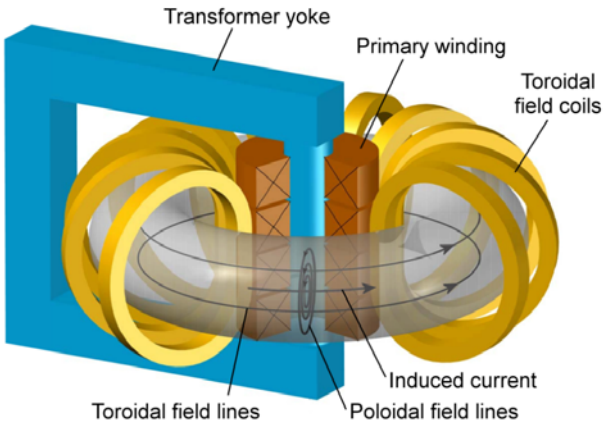

Fig. 1. Schematic drawing of a tokamak-type magnetic trap. The toroidal vacuum chamber and additional coils (used to form the poloidal magnetic field) are not shown.

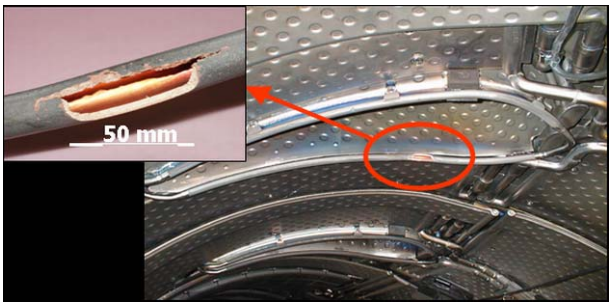

Fig. 2. Damage at the edge of the diagnostic port in the vacuum chamber of TORE-SUPRA device, caused by high--energy electron streams [19].

The toroidal electric field leads also to the generation of the so-called runaway electrons [15–17], since for electrons of sufficiently high energy the friction force due to collisions with plasma does not compensate the externally induced electrical force. Therefore, some electrons may be continuously accelerated and "run away" in the phase space, eventually escaping from the magnetic trap. Studies of the runaway electrons are motivated by several arguments:

– Runaway electrons can influence the plasma behavior since they can carry a substantial part of the plasma current.
– Such fast electrons propagate practically in a collisionless manner and they may act as suitable probes for the investigation of the non-collisional transport in tokamaks.
– In general they may improve the confinement of plasma and their interaction with waves may result in a transfer of energy to plasma, but interaction of streams of highly energetic electrons with the internal walls of the vessel may result in severe damages of fusion facilities.

In fact, during tokamak experiments, e.g. within the TORE-SUPRA facility in Cadarache (France) [19, 21], a significant damage of the cooling ducts in the vicinity of the diagnostic port had been observed, as presented in Fig. 2.

For these reasons the phenomenon of high-energy runaway electrons has been a subject of extensive theoretical and experimental studies at several plasma research centers. The main aim of this invited paper is to describe possible mechanisms by means of which such fast runaway electrons might be generated and to discuss various diagnostics methods which might be useful in experimental studies of this effect.

Generation of fast electrons in tokamaks

In order to describe the process of generation of fast electrons let us consider a poloidal cross-section of a tokamak-type trap, and in particular the magnetic surface and a displacement of the electron orbit, as shown in Fig. 3.

Electrons are driven by the force due to the induced electric field $\vec{F}_e = -e\vec{E}$. They are also subject to the drag force resulting from Coulomb interactions with plasma ions, $\vec{F}_d = m_e\vec{u}_e\nu_{\text{coll}}$, where ν_{coll} is the collision frequency. For a non-relativistic electron moving faster than thermal electrons (but at $u_e \approx u_{th}$) and for a Maxwellian

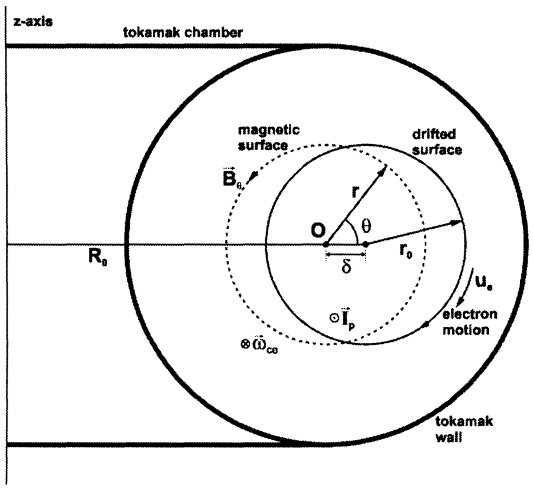

Fig. 3. Cross-section of a tokamak chamber and the displacement δ of the electron orbit.

distribution one can use a simple formula

$$(1) \qquad \nu_{\text{coll}} = (e^4 n_e \ln\Lambda / 4\pi\varepsilon_0^2 m_e^2 u^3)(2 + Z_{\text{eff}})$$

where e is the electron charge, n_e is the electron number density, $\ln\Lambda$ is the Coulomb logarithm, ε_0 is the vacuum permittivity, and Z_{eff} is the effective charge number of ions.

Production of runaway electrons

For electrons moving with the speed much larger than thermal speed, $u_e >> u_{th}$, the drag force may be expressed as the change of the parallel component of the momentum due to collisions

$$(2) \quad F_d = (\Delta p_{\Uparrow} / \Delta t_{\text{coll}}) = \left[dW / ds - 0.5 m_e u_e{}^2 \gamma (d\Theta^2 / dx) \right]_{\text{coll}}$$

where $W = (c^2p^2 + m_e^2c^4)^{1/2}$, $\Delta x = u\,\Delta t$, γ is the relativistic factor, and $\Theta = u_\perp/u_{\Uparrow} \approx p_\perp/p$ if the pitch angle is assumed to be much smaller than 1. In Eq. (2) the first term (dW/ds – the stopping power) describes the electron energy loss, while the second term describes the pitch angle scattering of the electron.

Considering electron-ion collisions and electron--electron collisions separately, one can calculate the drag force by averaging both contributions. Finally one gets

$$(3) \qquad F_d = -(e^4 n_e \ln\Lambda / 4\pi\varepsilon_0^2 m_e^2 u^2)[1 + (Z_{\text{eff}} + 1)/\gamma]$$

where $\ln\Lambda = \ln(\Theta_{\max}/\Theta_{\min})$, $Z_{\text{eff}} = \Sigma_i n_i Z_i^2/n_e$. It should be noted that the term $(Z_{\text{eff}} + 1)/\gamma$ gives negligible contribution at higher energies.

The condition that the drag force is equal to the driving force of the electric field $F_d = F_e$, defines a critical speed for the electrons

$$(4) \qquad u_{\text{crit}} = \left[e^3 n_e \ln\Lambda (2 + Z_{\text{eff}}) / 4\pi\varepsilon_0^2 m_e^2 E \right]^{1/2}$$

which corresponds to the critical energy $W_{\text{crit}} = (1/2)\, m_e u_{\text{crit}}^2$, that may be described by a simple formula

(5) W_{crit} [keV] = 2.2 (2+ Z_{eff}) n_e [10^{19} m^{-3}] / E [V/m]

as long as $W_{crit} >> T_e$.

Any thermal electron will run away if the electric field is higher than the critical value

(6) E_{crit} [V/m] $\approx 4 Z_{eff}\, n_e\, (10^{19}\ \mathrm{m}^{-3})/T_e$ [keV]

When the electric field remains smaller than E_{crit} the distribution function is close to a Maxwellian and only a small number of electrons can run away.

The considerations given above concern a behavior of a test electron in plasma. In order to obtain a kinetic description of the electron population one must solve the Fokker-Planck equation to find the actual electron distribution function. Then one can compute the runaway production rate, i.e. the number of runaway electrons which acquire velocities exceeding u_{crit}. It should be noted, however, that very fast runaway electrons (of energies exceeding 20 MeV) decouple from the bulk electrons and their behavior is similar to that of the test particles.

A more detailed analysis should take into account the fact that the orbit of a runaway electron in a tokamak is shifted from the magnetic surfaces due to the curvature and gradient-B drifts, as shown in Fig. 3. The motion of a runaway electron consists of three components:

1. The gyrotron rotation around the magnetic field lines $\omega_{ce} = eB/\gamma m_e$, where $\gamma = (1 - u^2/c^2)^{1/2}$ with the Larmor motion $\rho_{eL} = \gamma m_e u_\perp / eB$ and the velocity $u_\perp$.
2. The helical motion of the guiding center along the field lines

(7) $\vec{u}_{\Uparrow} = u_\Phi \vec{k}_\Phi + (u_\Phi B_\Theta / B_\Phi)\vec{k}_\Theta - (u_\Phi B_z / B_{\Phi u})\vec{k}_z$

where $\vec{k}_\Phi$, $\vec{k}_\Theta$ and $\vec{k}_z$ are unit vectors in the toroidal, poloidal and vertical direction, respectively.

3. The drift of the guiding center, due to the curvature and the gradient of the magnetic field

(8) $\vec{u}_d = \left[(u_{\Uparrow}^2 + u_\perp^2 / 2) / R\omega_{ce} \right] \vec{k}_z$

The $E \times B$ drift is here neglected because it is usually much smaller than the other terms. Now let us consider the conservation of toroidal angular momentum

(9) $J_\Phi = \gamma m_e R u_\Phi - e\Psi(r)$

where $\Psi(r)$ is the poloidal magnetic flux

(10) $\Psi(r) = \int_0^r B_\Theta r dr = (\mu_0 R_0 / 2) \int_0^r dr'' / r'' \int_0^{r''} j(r') dr' r'$

and $j(r')$ denotes the current density. Hence $d(\gamma m_e R u_\Phi) = eB_\Theta R dr$, where $dr = \delta$ is the displacement considered above. During every poloidal cycle the electron kinetic energy $W = p^2/2\gamma m_e$ and the magnetic momentum $\mu = p_\perp^2/2\gamma m_e B$ are constants of motion. The toroidal momentum is $p_\Phi = \gamma m_e u_\Phi \cong (W - \mu B)^{1/2}$ and $dB/B = dR/R$. Hence, one can write $\delta = dr = (1/e\, B_\Theta R)\, d(p_\Phi R)$, which gives

(11) $\delta = (p_\Phi / eB_\Theta R)\ (1 + p_\perp^2 / 2p_\Theta^2)\ dR$

For runaway electrons $p_\Phi >> p_\perp$ and for a single cycle one obtains after averaging $dR \cong r$. Hence $\delta \cong qp_\Phi / eB_\Theta R$ where $q = \langle r/B_\Theta \rangle B_\Phi / R$ is the average safety factor. We should also take into account that for electrons displaced from the magnetic axis (see Fig. 3) the Lorentz force (due to the poloidal magnetic field) must be balanced by the centrifugal force $\gamma m_e u_\Phi^2 / R = e u_\Phi B_\Theta$. The poloidal projection of the orbit may be approximated by a circle, where the electron moves with the velocity $u_\Theta = u_\Phi B_\Theta / B_\Phi$ and a drift velocity u_d. From the schematical drawing shown in Fig. 3 we deduce that $dx/dt = -u_\Theta \sin\Theta$ and $dr/dt = u_d \sin\Theta$. Hence, the considered circle centered at $x = \delta$ is described by the equation

(12) $dr/dx = -u_d / u_\Theta \cong u_\Phi B_\Phi / R\ \omega_{ce} B_\Phi \cong \delta / r$

In a more precise treatment of the runaway orbits for different current distributions one must take into account the effect of the electric field and an increase in the energy of the runaway electrons [28]. In fact, for runaway electrons of very high energy the drift orbits are no longer closed and such electrons escape from plasma before the drift surface touches the limiter.

The condition for the maximum value of the energy of electrons that remain confined may be expressed by the formula

(13) W_{max} [MeV] $\cong (R_0 I_p c / a I_A u_{\Uparrow}) B_\Theta\ (r^*) / [1 + s'(a)] B_\Theta(a)$

where $I_A = 4\pi m_e c / \mu_0 e = 17$ kA is the so-called Alfvén current, $r^* = r - s(r)$, $s(r)$ is the Schafranov shift between the geometrical center and the center of the magnetic flux surface, and $s'(r)$ is the derivative of this shift at the plasma boundary (depending on the pressure and current profiles).

On the basis of the relations given above computations of the maximum electron energy values for the TEXTOR experiment in Jülich, Germany, were performed many years ago [12, 13], as shown in Fig. 4.

One can easily see that depending on the density profile, the maximum energy of fast electrons at $r/a = 0.6$ can reach from 40 to 120 MeV. It should be noted, however, that although the electrons exceeding the critical velocity may be accelerated continuously, in practice their energy is limited by several factors:

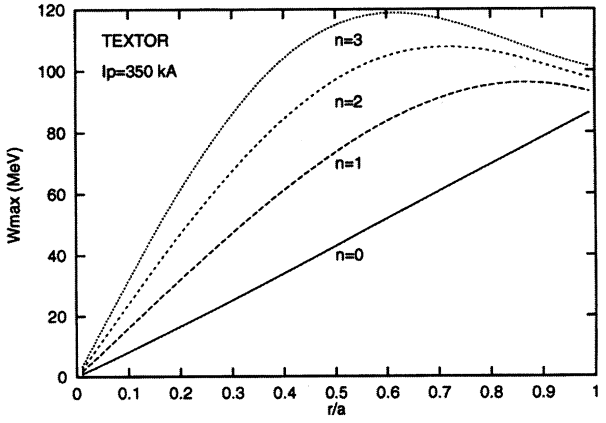

Fig. 4. Values of W_{max} computed for the TEXTOR device, assuming different plasma density profiles [12], which were characterized by the term $[1 - (r/a)^2]^n$.

the synchrotron radiation, an orbit shift, a time limit, magnetic field ripples and instabilities.

As regards the synchrotron radiation its total power can be expressed as $P_s = 2r_e m_e c^3 \gamma^4 / 3R_{curv}^2$, where r_e is the classical electron radius, and R_{curv} describes the helical orbit described by the formula

$$1/R_{curv} = (1 - \Theta^2)/R_0 + eB_\Theta/m_e c\gamma \tag{14}$$

where the pitch angle $\Theta = u_\perp/u_\Uparrow$. Equating this power loss to the power absorbed from the electric field $P_{gain} = ecV_{loop}/2\pi R_0$ one can estimate the maximum attainable γ_{max}. For example, in the case of TEXTOR one should substitute $V_{loop} = 1$ V, $R_0 = 1.75$ m, $B = 2.25$ T and $\Theta = 0.12$, which gives $W_{max}^{synch} = 25$ MeV. It should be noted that higher values can be obtained during a disruption when the loop voltage is much larger.

Considering the orbit shift, the displacement δ of the runaway orbit from the magnetic surface can be expressed by

$$\delta \cong qp_\Phi/eB_\Phi R \cong qW/ecB_\Phi \tag{15}$$

where $q = <r/B_\Theta> B_\Phi/R$ is the average safety factor. Hence $W_{max}^{shift} = aecB_\Phi/q_a$; for TEXTOR (where $q_a = 3.8$, $I_p = 350$ KA) we obtain $W_{max}^{shift} \cong 80$ MeV.

As regards the time limit, if the radiation losses are neglected, the maximum energy to be reached by a runaway electron in a single loop may be estimated from a simple formula

$$W_{max}(t) = ec \int V_{loop}\, dt/2\pi R_0 \tag{16}$$

Hence, for the TEXTOR one gets $W_{max}(t) = 27\Phi(t)$ MeV, where $\Phi(t)$ is the flux swing applied to plasma. In particular, $\Phi(t) = 0.8$ at $t = 0.6$ s.

Considering magnetic field ripples, at the finite number of coils N the toroidal magnetic field is modulated and its modulation frequency is $\omega = nNc/R_0$, where n means the harmonic number. A theoretical analysis showed that if the electron cyclotron motion is in resonance with the field modulation frequency the electrons are scattered effectively [18]. Therefore, depending on the harmonic resonance and an amplitude of the field ripple, an energy limit for the runaways may be expressed as

$$W_{max}^{ripple} = eBR_0/nNm_e c \tag{17}$$

Hence, for TEXTOR one gets $W_{max}^{ripple} = 70/n$ MeV and the second harmonic ($n = 2$) seems to be of importance.

As regards an influence of instabilities, free energy (due to the non-Maxwellian part of the electron distribution function) may be exchanged between electrons and plasma oscillations. When a certain threshold is exceeded, instabilities occur which limit the energy or confinement properties of runaways.

Transport of runaway electrons

Processes of the energy and particle transport in fusion plasmas are still poorly understood and they are a subject of extensive studies. A cross-field transport in tokamaks is governed by several processes:

1. The collisional transport, which is described as a classical transport in cylindrical systems and a neo-classical one in toroidal configurations. In fact, the neo-classical runaway diffusion coefficient is estimated to be very small.
2. Transport induced by electrostatic fluctuations. In general, turbulent fields can increase the $E \times B$ transport if the density fluctuations are in phase with the electrostatic fluctuations, but for runaway electrons this transport may also be neglected.
3. Transport induced by magnetic fluctuations. It is evident that runaway electrons can diffuse because they travel along the fluctuating field lines, which diffuse themselves. Unfortunately, this process has not so far been described quantitatively and there are some old estimates only [24].

In small tokamaks the generation of runaway electrons is usually caused by the so-called Dreicer mechanism of the electron acceleration [22] and the runaway production rate can be expressed as:

$$\lambda_R \sim C(Z_{eff})\varepsilon^{-3(Z+1)/16} n_e \nu_e \exp\{-1/4\varepsilon - [(Z+1)/\varepsilon]^{1/2}\} \tag{18}$$

where C is the proportionality coefficient, Z_{eff} is the effective ion charge, $\varepsilon = E_0/E_{DR}$ and the Dreicer critical field is given by

$$E_{DR} = e^3 \ln \Lambda n_e Z_{eff} / 4\pi\varepsilon_0^2 T_e \tag{19}$$

while the electron collision frequency is equal to

$$\nu_e = 2.91 \times 10^{-6} \ln\Lambda\, n_e Z_{eff} T^{-3/2} \tag{20}$$

It can be easily seen that a considerable increase in the plasma density – as had been observed in different experiments, e.g. up to $<n_e> = (7\text{–}10) \times 10^{18}$ m^{-3} in the ISTTOK device in Lisbon [22], – would result in the decrease of the runaway production rate by orders of magnitude.

Production of ripple-born electrons

It has already been mentioned above that due to the fact that there is only a finite number of toroidal coils in a tokamak, the magnetic field is not totally axisymmetric. There appear ripples in the magnetic field with the period of $2\pi/N$, where N is the number of the toroidal field coils (see Fig. 1). The appearance of magnetic field ripples has important consequences for the confinement of energetic charged particles. Significant losses of fast ions may occur if the ripples have sufficiently large amplitude [26]. Future nuclear fusion reactors would have to rely on the heating provided by the energetic alpha particles arising from fusion. Therefore, ripple losses are potentially an important problem for fusion reactors. The ripple losses tend to be localized and can therefore cause severe damage in limited areas of plasma facing components. An example has been presented in Fig. 2, and another case is shown in Fig. 5.

In the TORE-SUPRA experiment described earlier the facility was equipped with an inboard limiter which

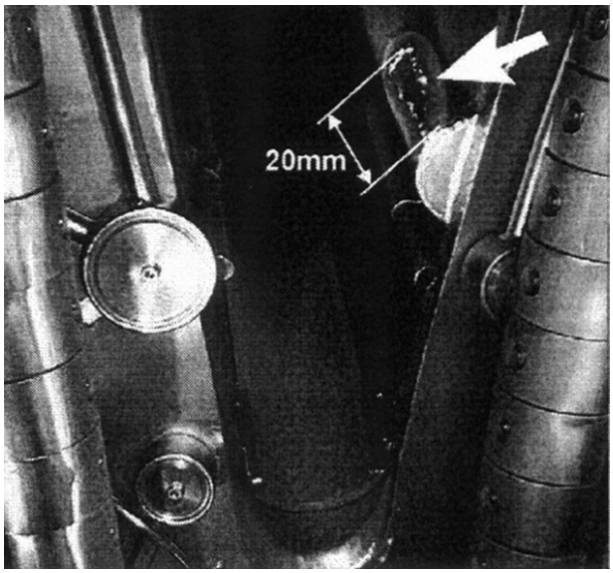

Fig. 5. Perforations of a pumping duct in the upper vertical port, caused by fast runaway particles [19].

was fully toroidal, constituting a broad poloidal belt made of graphite or CFC (carbon fiber composite) tiles. The detailed theoretical analysis of the field configuration has shown that some fast ions that were initially trapped in the TORE-SUPRA field, could nevertheless escape in the upward direction (and some fast electrons too – in the downward direction), as shown in Fig. 6.

The toroidal magnetic field of the TORE-SUPRA tokamak displayed relatively large ripples, i.e. large value of $(\delta B/B)$, which increased to about 7% at the plasma edge low field side (at $r/a = 1$). Therefore, a large fraction of the plasma volume was affected by particle trapping in local magnetic ripple wells (due to the pitch angle scattering). Those particles (ions and electrons) could escape from the plasma core along so-called *iso-B* lines. In the previous TORE-SUPRA configuration fast ions and electrons, which were accelerated during LHH or ICRH up to 100–300 keV energy, could drift upward and downward, correspondingly. In fact the fast runaway electrons were routinely observed in TORE-SUPRA during disruptions (via hard X-ray and neutron monitors, as well as synchrotron radiation and wall heating recorded with IR cameras) [20].

It should here be mentioned that to reduce ripples without using an unacceptably large number of the toroidal field coils one may apply a method based on the use of appropriate ferritic inserts, which had been researched and developed at the JFT-2M facility. In that case the fundamental mode ripple was reduced down to 0.07% [14].

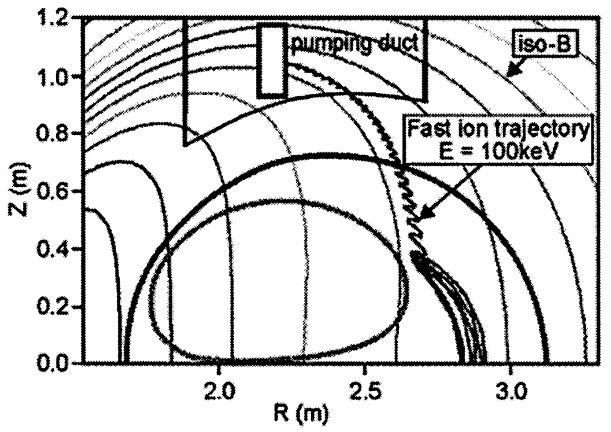

Fig. 6. Trajectory of a fast ion escaping from the former TORE-SUPRA field [3].

Diagnostics of the fast electrons in tokamaks

The emission of fast electrons escaping from tokamak devices had been studied in numerous experiments. The use was made of different diagnostic techniques, an incomplete list of which is given below:

1. An indirect method based on measurements of secondary X-rays.
2. Another indirect method based on measurements of secondary neutrons.
3. Measurements of the synchrotron radiation.
4. A new immediate method based on the use of Cherenkov-type detectors.

The first three methods have been applied in different laboratories for many years, but they cannot deliver accurate information about regions of the fast electrons emission. The adaptation of the Cherenkov--type detectors for instantaneous and local measurements of the fast electrons in tokamaks was for the first time proposed by the present author in 2004 [25]. All these diagnostic techniques will be described in detail in subsequent subsections.

Measurements of secondary X-rays

In hot plasmas processes leading to the production of secondary X-rays or gammas are as follows:

1. The bremstrahlung from the plasma. For runaway electrons the collision frequency becomes very low, but fast electrons undergo Coulomb interactions with plasma ions, which result in the emission of photons having a continuous energy spectrum up to the kinetic energy of the incident electrons.
2. The bremstrahlung from the limiter. When runaway electrons strike a solid state limiter, they are slowed down and emit a continuous spectrum of photons.
3. The production of electron-positron pairs. Collisions of energetic runaway electrons with nuclei can in principle produce electron-positron pairs (for electron energies above the natural energy threshold equal to 1.02 MeV), but for the typical tokamak experiments the cross-section of this process is too low to allow for the effective detection. Therefore only two bremstrahlung mechanisms may play any role.

Measurements of secondary neutrons

The processes in high-temperature plasmas leading to the production of neutrons can be listed as follows:

1. The electro-disintegration. Energetic electrons in plasma can interact directly with plasma ions and split them apart; in the case of deuterium plasma this results in the emission of neutrons (from primary deuterons). The energy threshold of this process amounts to a few MeV.

2. Photo-nuclear processes (γ, n) and subsequent radioactive decays. Energetic photons emitted by the fast electrons interacting with plasma ions or solid limiter can stay inside the limiter material and cause photo-nuclear processes. If the photon energy is high enough to cause a breakup a stable nuclei, it can cause the emission of neutrons and photons; for example in the case of carbon the energy threshold of the primary photon for the neutron emission is about 10 MeV. A residual nucleus may become radioactive and the analysis of the limiter material can provide an information about energies of impinging electrons [1].

To measure secondary gammas and neutrons in the TEXTOR device the use was made of a detector containing the NE-213 liquid scintillator. The detector head was aligned tangentially or radially to the plasma current direction. The measuring system was operated with counting rates up to 3×10^5 s^{-1}. The complete n/γ discrimination was achieved for electrons with energies above 0.1 MeV and protons with energies exceeding 0.8 MeV. The pulse height (energy) resolution was about 8% for 2.5 MeV protons [4].

From the above information it is clear that to determine the origin of the observed radiation one must measure X-rays, neutrons and their energies. Such measurements are usually carried out by means of scintillation detectors, in which an impinging photon produces Compton scattered electrons, and an impinging neutron generates recoil protons. These charged particles excite molecules of the scintillation material, which emit fluorescence radiation measured by a photo-multiplier. In order to identify photon- and neutron-induced events one can apply a pulse shape analysis.

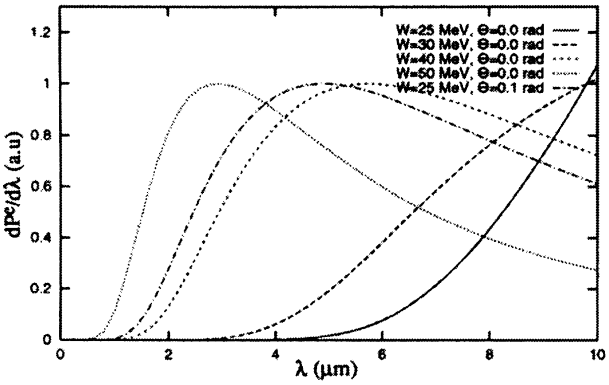

Fig. 7. Normalized synchrotron spectrum of one electron for different W and Θ values [13].

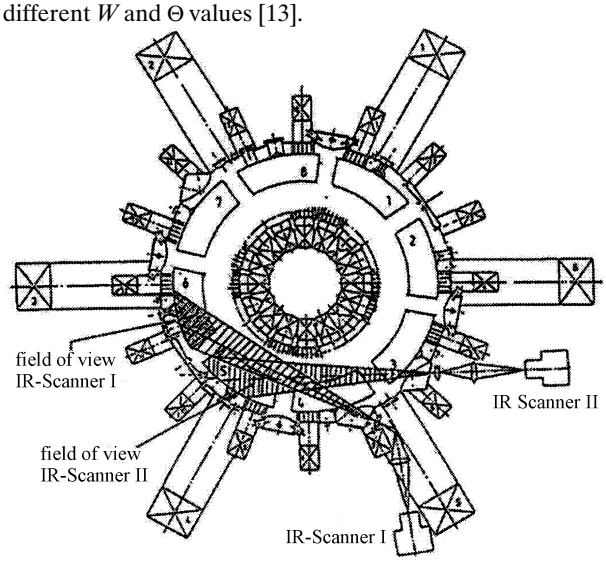

Fig. 8. Experimental arrangement of IR cameras at the TEXTOR facility [12].

Measurements of the synchrotron radiation

The electromagnetic radiation emitted by the bulk electrons (not the relativistic ones) gyrating in the magnetic field is called the cyclotron emission (ECE) at the gyration frequency. The radiation of the second harmonic is often employed in many contemporary tokamaks to determine the electron temperature. It should be added that in the nuclear fusion literature the higher harmonics of the cyclotron radiation, which are generated mostly by slightly relativistic electrons ($W_{\text{kin}} < m_e c^2$), are also called the synchrotron radiation.

If $W_{\omega\phi\psi}$ is the energy emitted by a relativistic electron moving along a circular orbit per unit angular frequency interval ($d\omega$) and per unit solid angle ($d\Omega = d\psi\, d\phi$) the detected power $d^2P_e/d\Omega d\omega$ may be found by multiplying $W_{\omega\phi\psi}$ by the repetition frequency $c/2\pi R$. After appropriate substitutions and integration over all frequencies we obtain

$$(21)\quad dP_e/d\Omega = ce^2\beta^4 [(1 - \beta\cos\Theta)^2 - (1 - \beta^2)\sin^2\Theta \sin^2\phi] /4\pi\varepsilon_0^4\pi R^2 (1 - \beta\cos\Theta)^5$$

In the orbital plane ($\phi = 0$) at the width of the aperture equal to $\delta = 1/\gamma$ one can draw a normalized synchrotron spectrum of one electron as a function of $\gamma\cos\Theta$. Then the total power radiated by an electron is equal to $P_e = 2r_e m_e c^3 \beta^4 \gamma^4 / 3R^2$, where $r_e = e^2/4\pi\varepsilon_0\, m_e c^2 = 2.82 \times 10^{-15}$ m is the classical electron radius. Hence, one can draw $dP_e/d\lambda$ vs. the wavelength λ, as shown in Fig. 7.

In order to record the synchrotron emission within the middle infrared (IR) spectral range the use can be made of a thermo-graphic camera viewing the plasma tangentially in the direction of electron approach. Such measurements have been carried out, e.g., in the TEXTOR experiment [12], as shown in Fig. 8.

Some examples of the IR images, as recorded in the TEXTOR experiment, are presented in Fig. 9.

Important information may be obtained from time-resolved measurements [20], as shown in Fig. 10.

Other examples, which show results from the TORE-SUPRA experiment [20], are presented in Fig. 11.

In the first example the central electron temperature T_e, as measured from ECE, dropped in less than

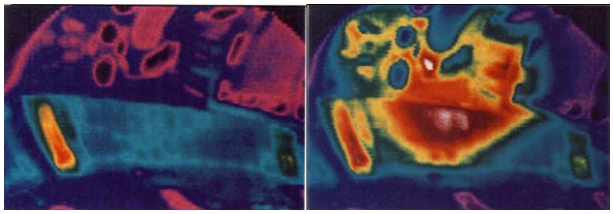

Fig. 9. Image of the thermal radiation from the TEXTOR limiter (left, taken at $t = 0.5$ s) and that of the synchrotron radiation (right, recorded at $t = 1.5$ s) [12].

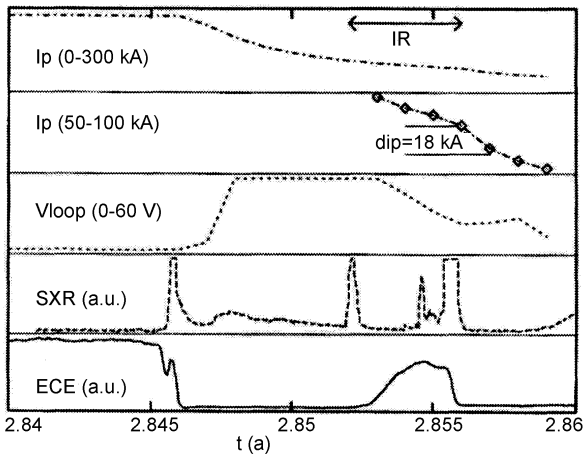

Fig. 10. Typical time-resolved signals recorded during the disruption within TEXTOR. Traces from top to bottom: The discharge current (I_p), the extended current trace, the loop voltage (V_{loop}), the soft X-ray radiation (SXR) and the ECE. The period of the synchrotron emission is indicated by the arrows (IR) [20].

1 ms. After a short spike the discharge current started to decrease and plasma was pushed towards the inner wall. During the ramp down a large neutron signal was observed, which was about 100 times higher than that from the plasma phase. Those neutrons were produced by fast electrons accelerated to energies exceeding 10 MeV. In the second case the current fell and the movement of plasma stopped temporarily, as a result of the stabilization of a runaway current by the vertical

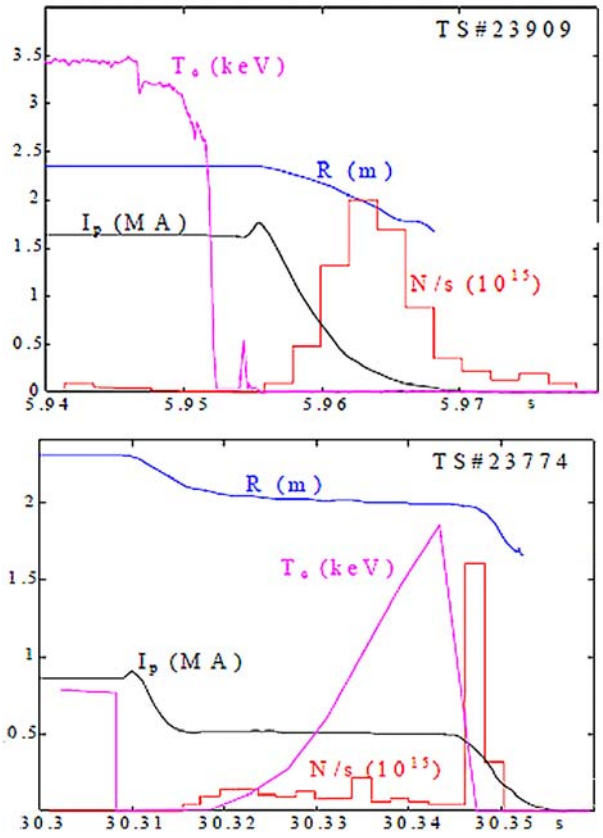

Fig. 11. Waveforms recorded for a typical disruption in the TORE-SUPRA (top) and those from another shot with a disruption exhibiting a runaway plateau (bottom) [20].

field, and a large non-thermal ECE radiation appeared. It was observed that duration of such a plateau can vary from a very short to above 1 s.

Energies of the runaway electrons can be determined by the correlation of two diagnostic techniques, i.e. the photo-nuclear activation (with a high threshold) and neutron/electron ratio. It is evident that the energy determination is very important for the verification of different runaway creation and acceleration models. In the tokamak experiments mentioned above there two main mechanisms were considered:

1. The so-called Dreicer mechanism, when a large number of runaway electrons is created at the very beginning of the current quench and accelerated continuously at an energy gain of about 60 MeV/MA. In such a case the energy distribution should be close to monotonic one.
2. An avalanche mechanism, when a small population of electrons grows exponentially via head-on collisions with the cold plasma electrons. In that case one can predict a Maxwellian distribution with a temperature reaching up to 10–15 MeV.

The first photo-activity measurements within the TORE-SUPRA were based on spallation reactions of bismuth (Bi), which have thresholds from about 30 to about 50 MeV. The Bi samples were placed outside the vacuum chamber in the hard X-ray stream produced by fast electrons impinging upon the chamber inner wall [20]. Geometry of the irradiation was too complex to make possible absolute measurements, but several discharges were studied by recording γ-spectra from the irradiated Bi samples, as shown in Fig. 12.

Theoretical ratios for the selected Bi-isotopes were also calculated under assumption that the fast electrons are fully slowed down in graphite tiles. The main aim was to find whether the recorded Bi-isotope ratios correspond to fast monoenergetic electrons or those with a Maxwellian energy distribution.

Another diagnostic method, used to determine electron energies, was based on the estimate of the number of neutrons produced by each electron. In this approach it was assumed that the electrons are also stopped in the graphite tiles, but photo-nuclear processes occur in the SS (stainless steel) wall of the vacuum chamber. The analysis of two possible mechanisms (the Dreicer model and the avalanche approach) showed that the electron

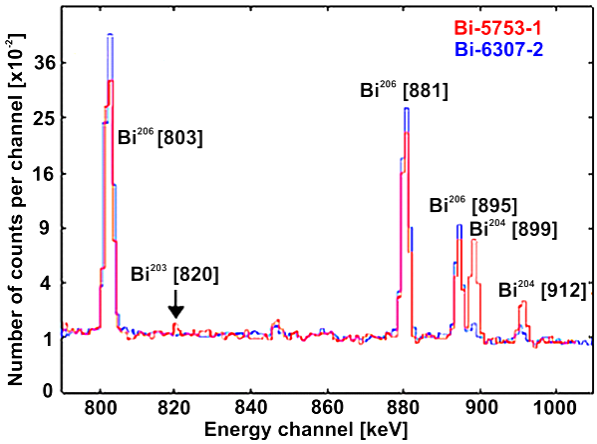

Fig. 12. Typical γ-spectra obtained from Bi samples irradiated within the TORE-SUPRA [20].

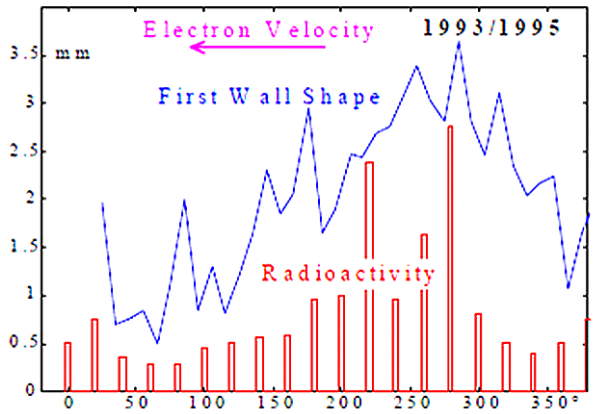

Fig. 13. Radioactivity measured in TS along the inner toroidal limiter in 1993–1995 experiments [20].

distribution functions should be described by different curves and the numbers of the produced neutrons should also be different. In the TORE-SUPRA experiments mentioned above the number of photo-neutrons was measured using the fission chambers, and the number of fast electrons was estimated under assumption that the plateau current is fully carried by the runaway electrons. The results showed that the avalanche process dominated during the current disruptions.

In the early TORE-SUPRA experiments most of the runaway electrons were lost in the equatorial plane, upon the toroidal belt limiter placed at the high field side. Radioactivity measurements along the inner toroidal limiter showed 18 distinct peaks which were correlated with the ripples due to coils, as presented in Fig. 13.

The observed angular variations were explained by a slight misalignment of 36 modules of the limiter. That conclusion was confirmed by changing positions of the modules in an appropriate way. The shadowing of the retracted modules by the neighboring ones was also observed.

According to the theoretical considerations presented above the production of runaway electrons recorded in the TORE-SUPRA experiments was weakly sensitive to the plasma density, but it varied strongly with the toroidal field. The Dreicer model was not applicable during strong plasma disruptions when the plasma parameters evolved very rapidly.

Measurements involving the Cherenkov-type detectors

As it was mentioned above, in order to determine the properties of fast electrons in tokamaks the author proposed to adapt the Cherenkov-type detectors [25]. It is well known that the Cherenkov radiation appears when a charged particle penetrates a transparent medium with the velocity (u) higher than the phase velocity of light (u_l) in this medium [29]. The phase velocity of light is $u_l = c/n$, where n is the refractive index of the medium. The condition may be written as $u > u_l$ or $\beta n > 1$ where $\beta = u/c$. From this relation one can easily see that there is an energy threshold for the emission of the Cherenkov radiation. The minimal electron energy required to generate the Cherenkov radiation is given by

$$E_{\min} = E_0/(1-\beta^2)^{1/2} - E_0 \tag{22}$$

where $E_0 = 511$ keV is the electron rest energy.

The emitted energy increases with an increase in a particle velocity and it is larger for a medium with a larger refractive index. In the polar coordinates (z, ρ, θ) the charged particle can emit the conical electromagnetic wave described by the formula

$$A \sim e^{i\omega\left(t-\frac{z\cos\theta+\rho\sin\theta}{u}\right)} \tag{23}$$

and at $\beta n > 1$ the Cherenkov radiation can be emitted within at an angle θ to the direction of the particle motion. Energy of the Cherenkov radiation (per unit length of path) may be expressed as

$$\frac{dW}{dl} = \frac{e^2}{c^2}\int_{\omega_1}^{\omega_2}\left(1-\frac{1}{n^2(\omega)\cdot\beta^2}\right)\omega\cdot d\omega \tag{24}$$

and for a unit length and the chosen wavelength interval ($\lambda_1 - \lambda_2$) one gets

$$\frac{dW}{dt} = 2\pi^2 e^2\,\frac{\lambda_2^2-\lambda_1^2}{\lambda_2^2\cdot\lambda_1^2}\left(1-\frac{1}{\beta^2 n(\lambda_1)\cdot n(\lambda_2)}\right) \tag{25}$$

This means that e.g. for a charged particle moving with $\beta \approx 1$ the energy loss within the visible interval from $\lambda_1 = 3000$ Å to $\lambda_2 = 6000$ Å would be equal to 1.7 keV/cm, while the ionization losses for such a particle would be about 2 MeV/g/cm^2.

It should be noted that the most characteristic features of the Cherenkov radiation are as follows:
- a low-energy threshold,
- the directional character,
- an almost instantaneous emission (with delay $< 10^{-9}$ s),
- the intensity about 2–3 orders higher than that of the typical bremsstrahlung [29].

Because of these features detectors of the Cherenkov type are of particular interest for immediate and local measurements of fast electrons. In fact Cherenkov-type detectors may be used to study the emission of fast electrons above the determined low-energy threshold, which depends on the applied radiator, as shown in Table 1.

The Cherenkov detectors have been also for many years successfully used in studies of the fast electron beams emitted from high-current discharges in the plasma focus devices [7, 9]. Taking into account these advantages of the Cherenkov detectors the author's team has adapted this diagnostic technique also for measurements of fast runaway electrons in tokamaks.

Cherenkov measurements of fast electrons in CASTOR

The described diagnostic technique, based on the Cherenkov effect, was applied for the first time by the author's team in a CASTOR experiment in Prague, Czech Republic [11]. A simple one-channel measuring head had been designed, as shown in Fig. 14.

That Cherenkov probe was installed in one of the vertical diagnostic ports of the CASTOR toroidal chamber, as shown in Fig. 15.

Table 1. Basic parameters of some materials which might be used as Cherenkov detectors

Radiator material	Refractive index	Low-energy threshold for electron (keV)	Thermal conductivity ($W \cdot m^{-1} \cdot K^{-1}$)
Standard glass	1.80	104	1
Aluminium nitrade	2.15	66	170
Diamond crystal	2.42	51	2000
Rutile crystal	2.90	33	12

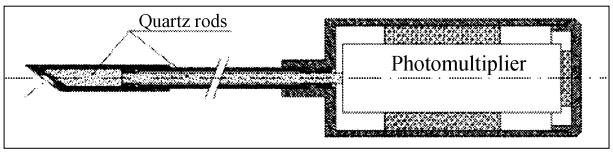

Fig. 14. Schematic drawing of the Cherenkov detector (not to scale) custom-designed for the CASTOR tokamak.

In a modified version of the Cherenkov detection system for the CASTOR the influence of hard X-rays on the photomultiplier signals had been eliminated, as shown in Fig. 16.

Measurements with different detector input orientations confirmed that the signals from the Cherenkov detector were induced by fast electrons, and electron-induced signals were recorded at different experimental conditions, as shown in Fig. 17.

It was found that the fast runaway electron emission in the CASTOR was strongly influenced by the toroidal magnetic field, and that this influence in the confined plasma region ($r_{Ch} \leq 70$ mm) was different from that in the limiter shadow ($r_{Ch} \geq 85$ mm) because variation of the magnetic field affects the particle confinement and plasma density, as shown in Fig. 18.

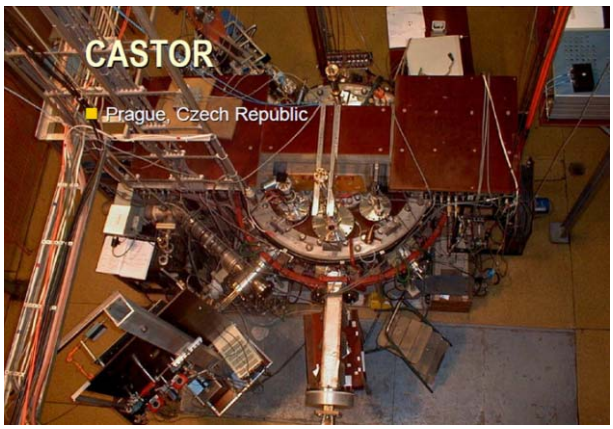

Fig. 15. Picture of the CASTOR experiment with the installed Cherenkov probe (photo by the IPJ team).

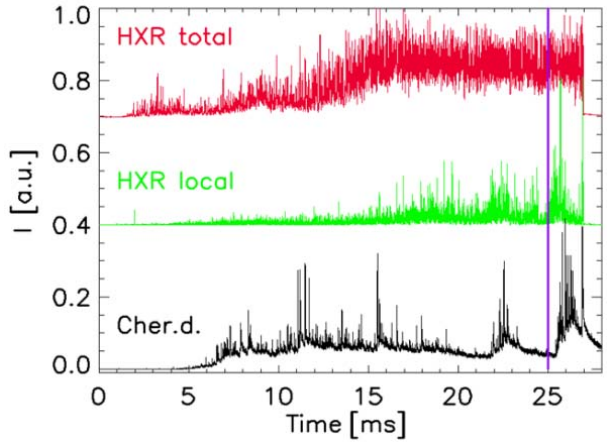

Fig. 16. Comparison of hard X-rays (HXR) and Cherenkov signals obtained from the CASTOR facility at $r = 60$ mm. The HXR-local signal was recorded close to the probe [8].

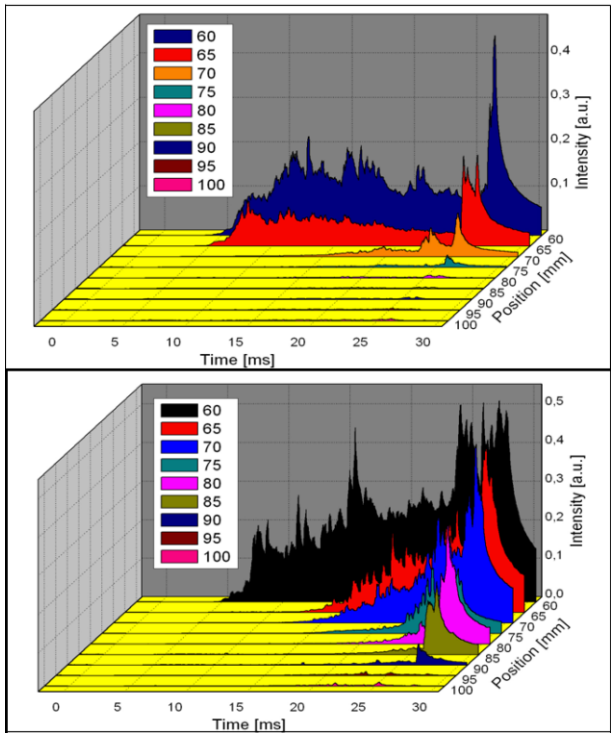

Fig. 17. Cherenkov signals as a function of the position of the Cherenkov detector head within the CASTOR device for high-density (top) and low-density discharges (bottom) [8].

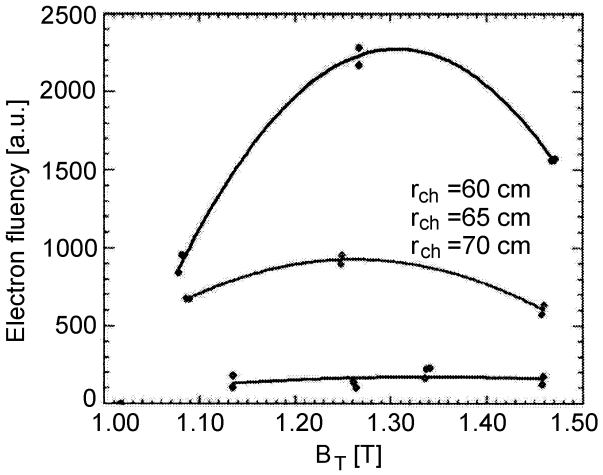

Fig. 18. Dependence of the electron beam fluency on the toroidal magnetic field B_T, as measured in the CASTOR tokamak for different radial position of the Cherenkov detector head [27].

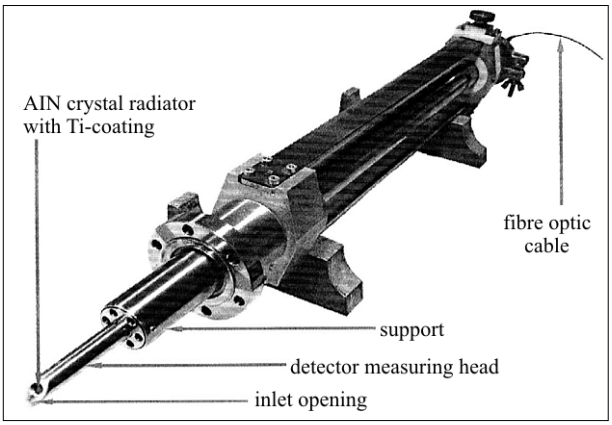

Fig. 19. Picture of a Cherenkov-type detector head with positioning equipment manufactured for ISTTOK [23].

Cherenkov measurements of fast electrons in ISTTOK

The next step in the IPJ team activity, aimed at the development of Cherenkov-type detectors for tokamak experiments, was the designing and manufacturing of a single-channel detector head for the ISTTOK device operated at Lisbon, Portugal [23]. In that case the use was also made of a AlN crystal, but the optical coupling of the Cherenkov radiator with a fast photomultiplier was realized by means of a fiber optic cable, as shown in Fig. 19.

The detector head was installed in the ISTTOK chamber, which is shown in Fig. 20.

The Cherenkov detector was placed at different distances from the toroidal axis of the ISTTOK chamber and the correlation of the Cherenkov signals with other experimental waveforms was investigated. An example of such signals, which were recorded when the detector was located at the radial position $r = 5.2$ cm, is presented in Fig. 21.

One can easily notice that the Cherenkov signals appeared at particular direction of the discharge current and the loop voltage only. Using this detector we were able to identify the runaway generation regimes in the ISTTOK tokamak. As a result the fluence of the runaway electrons with energies higher than 80 keV had been recorded. The numerical evaluation of the experimental data showed that such electrons might be generated in the vicinity of the plasma centre, and they could be detected at the location of the measuring probe.

Fig. 20. General view of the ISTTOK facility operated in Lisbon, Portugal (photo by the IPJ team).

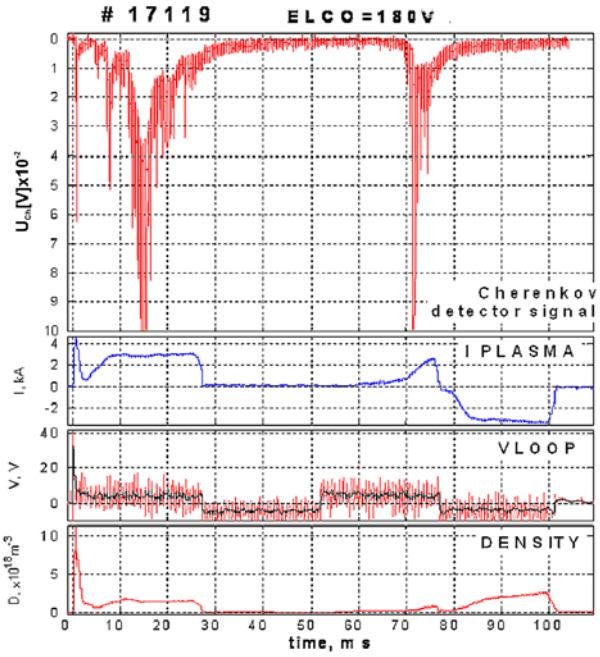

Fig. 21. Comparison of traces from the ISTTOK experiment: from top to bottom – signals from a Cherenkov detector I_{Ch}, the discharge current I_p, the loop voltage V_{loop}, and the average plasma density $<n_e>$ [23].

Fig. 22. Picture of a new four-channel Cherenkov-type detector head, designed and manufactured for ISTTOK experiments and installed within the positioning equipment [5].

For a new experiment with ISTTOK, in order to determine the energy spectrum of the fast electrons, the IPJ team designed and manufactured a four-channel Cherenkov detector head [5]. The probe had been equipped with four radiators made of AlN crystals 10 mm in diameter and 1 mm in thickness each, which were separated optically. Those radiators were shielded with molybdenum (Mo) coatings of different thickness. They were coupled with four fast photomultipliers through separate optical fiber cables. It made possible to record Cherenkov signals from electrons with energies above the threshold values, which were determined by the thicknesses of the applied Mo coatings. The new measuring head was mounted on the same positioning equipment, as shown in Fig. 22.

The new Cherenkov probe made it possible to record runaway electrons in different energy channels and compare the electron-induced signals with other waveforms, as shown in Fig. 23.

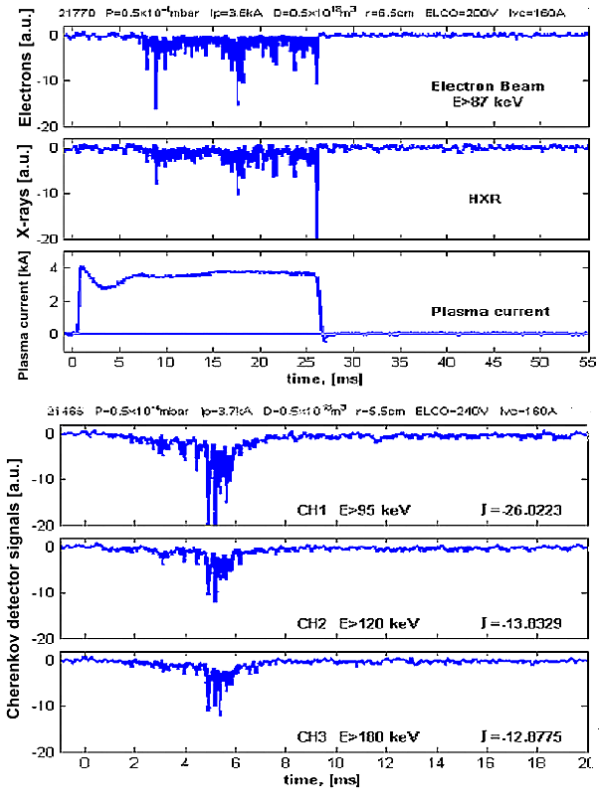

Fig. 23. Experimental data obtained from two ISTTOK discharges: from top to bottom – Cherenkov signals from electrons of energy > 87 keV, hard X-rays, plasma current, Cherenkov signals from different energy channels ranging from 95 to 180 keV. The time scales were different to identify instants of the runaway electrons emission more accurately [5].

The recorded Cherenkov signals were partially correlated with the hard X-rays (HXR), which were measured outside the tokamak chamber and were identified as bremstrahlung of fast electrons interacting with a limiter and metal walls. On the basis of detailed measurements it was possible to determine a dependence of the electron-induced signals on a distance of the Cherenkov detector from the toroidal axis of the ISTTOK chamber, i.e. to identify regions of the runaways emission, as shown in Fig. 24.

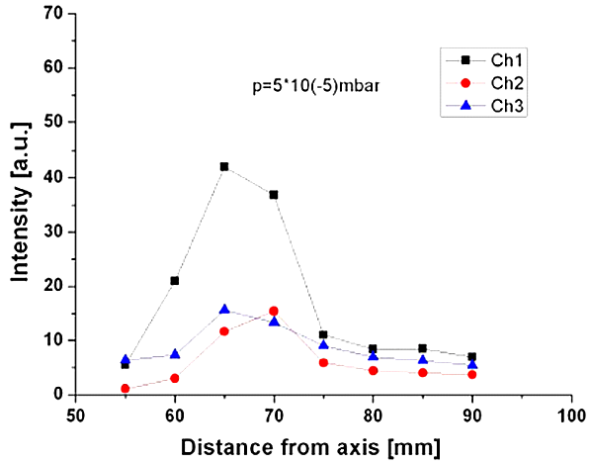

Fig. 24. Cherenkov-signal intensity as a function of a distance of the Cherenkov detectors from the ISTTOK toroidal axis. Electron energy thresholds of different channels were as follows: Ch1 > 69 keV, Ch2 > 95 keV, Ch3 > 119 keV [5].

It was also observed that, in spite of some differences in amplitudes, the HXR peaks (measured externally) and the Cherenkov signals (measured inside the tokamak chamber) were well correlated. It turned out that the diagnostic technique based the observation of the Cherenkov radiation appeared very useful for ISTTOK experiments. It should be noted, however, that credibility of the Cherenkov measurements at $R_{Ch} \leq 5.5$ cm was lower due to a possible influence the probe could have on the discharge parameters, e.g. plasma cooling and impurities release. Nevertheless, the applied technique made it possible to determine the plasma radius in ISTTOK within which the fast electron population appears and to learn what happens when the driving voltage and current intensity in the vertical magnetic coils are changed.

Cherenkov measurements of fast electrons in TORE-SUPRA

In fact the main aim of the EURATOM task, which (according to the author's proposal) was undertaken by the IPJ team, was to construct a Cherenkov-type probe for the TORE-SUPRA tokamak [2] in Cadarache, France, shown in Fig. 25.

Losses of fast ions and electrons from the TORE-SUPRA device had been investigated theoretically and experimentally for many years [2, 3], but a new diagnostic technique was needed. Acting on an invitation from the CEA-Cadarache, the IPJ team had performed a detailed analysis of the experimental conditions and designed a new Cherenkov-type probe [6, 10]. Taking into account high thermal loads which appear within the TORE-SUPRA tokamak, it had been decided to use a design with four diamond radiators with (Mo) coatings. The shapes of the diamond radiators and their holders (together with optical fiber cables) had been designed to reduce their thermal loads, as shown in Fig. 26.

In the designed probe all radiator surfaces were metal-coated except for small corners playing the role of optical contacts with the fiber cables. To transport the Cherenkov radiation the use was made of four separate optical cables attached to separate vacuum-feed-through connectors located inside the probe casing, as shown in Fig. 27.

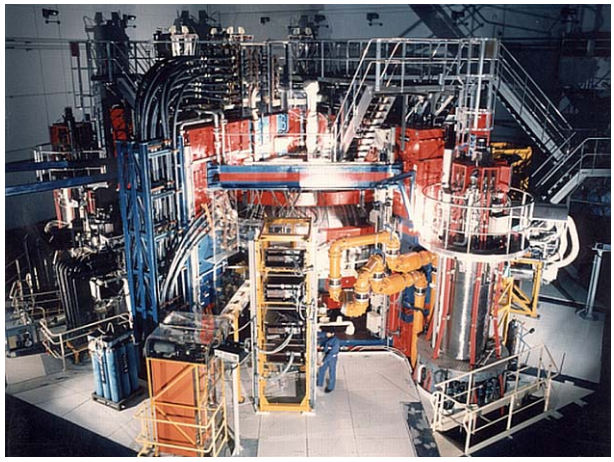

Fig. 25. General view of the TORE-SUPRA facility (http://www-cadarache-cea.fr).

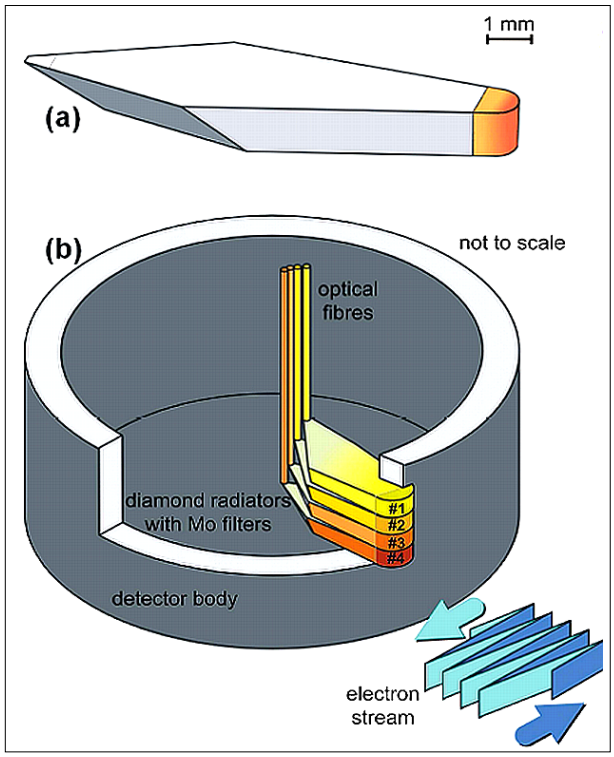

Fig. 26. Construction details of the Cherenkov-probe which was designed for TORE-SUPRA experiments [6].

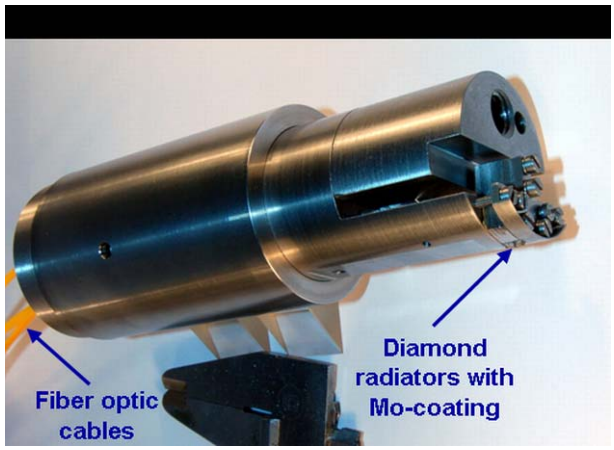

Fig. 27. Picture of the Cherenkov detector measuring head (without the outer CFC shield), which was manufactured for TORE-SUPRA experiments [10].

Internal supports of the radiators formed a good heat sink, and the whole probe was protected by an external CFC shield. The electron streams being probed could penetrate only front tips of the radiators which were shielded by Mo-coatings of various thicknesses. The use of the diamond radiators with Mo-filters of various thicknesses (10, 20, 50 and 100 μm) made it possible to detect electrons of different energies (> 84, > 109, > 173 and > 259 keV, respectively). In order to reduce overheating of the probe the use was made of a special fast moving shaft which could be introduced and withdrawn from a plasma region in about 30 ms. Therefore, in a single cycle of the shaft motion each radiator could record fast electrons twice (during inward and outward motion), as shown in Fig. 28.

The electron-induced Cherenkov signals had been recorded for the first time during the TORE-SUPRA

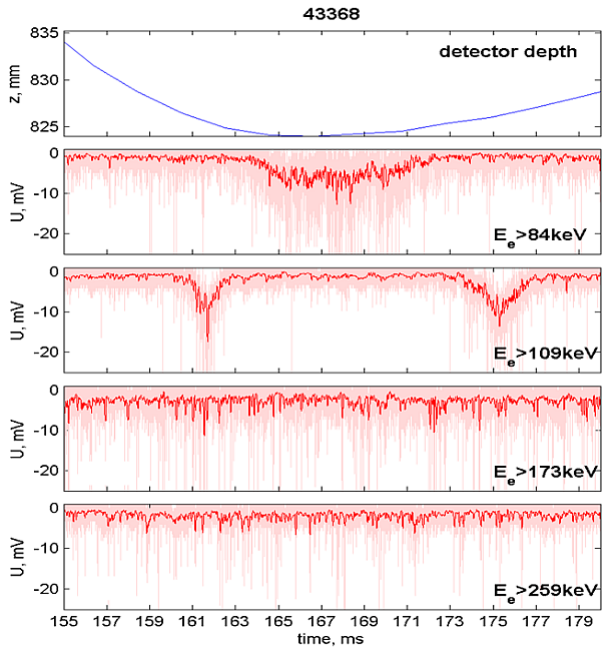

Fig. 28. Changes in the Cherenkov detector position and signals from different channels of that detector (four lower traces) for TS#43368 shot. The starting point of the time scale was chosen at $t = 4.2$ s [10].

discharges performed with an increased lower-hybrid (LH) heating [10]. A short operational cycle enabled the Cherenkov probe to be used twice during a single TS discharge. Knowing the characteristics of the probe motion it was possible to identify the positions of different radiators and to compare the Cherenkov signals obtained from different measuring channels, as shown in Fig. 29.

Those preliminary measurements in the TORE-SUPRA facility, which were carried out during several discharges with an increased LH and ICR heating, proved that the four-channel Cherenkov probe may successfully be applied for studies of fast electrons in a large tokamak experiment.

The analysis of the recorded Cherenkov signals showed that the fast electrons form a rather thin sheath within the scrape-of-layer (SOL) region and they appear when the level of LH and ICR heating is high

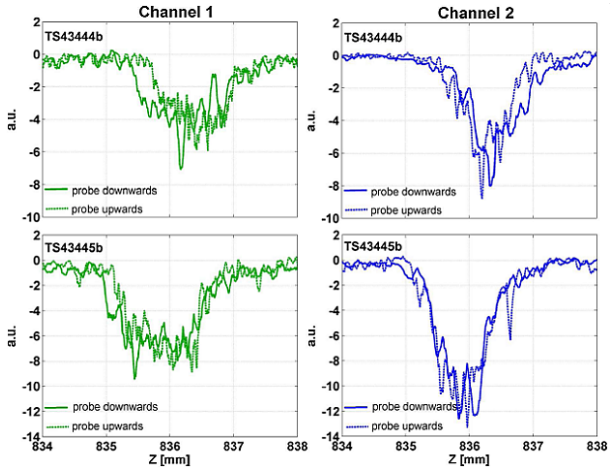

Fig. 29. Cherenkov signals from two measuring channels, as obtained from the second insertion of the probe (downwards and upwards) during two TS shots and converted into a dependence of signal amplitudes on the probe position [10].

enough. Power flux of such electrons may be very high and they can induce severe damages of plasma facing components (PFC) in tokamaks. Early information about generation of such powerful electron streams is of primary importance for controlling tokamak discharges. This is an example how important information may be gained from measurements of fast runaway and ripple-born electrons.

Summary and conclusions

The most important results of the studies presented in this paper may be summarized as follows:

- Different mechanisms of the runaway electrons generation have been described and compared. A particular attention was paid to two mechanisms: the so-called Dreicer mechanism and the avalanche mechanism.
- Various methods of passive diagnostics had been described for measurements of runaway or ripple--born electrons, which can escape from tokamaks, in particular the measurements of secondary X-rays, measurements of neutrons, measurements of the bremstrahlung radiation, and direct measurements with Cherenkov-type detectors. One must take into account the fact that each of these diagnostic techniques has its advantages and disadvantages.
- The Cherenkov-type detectors, as developed by the author's team, might be applied for studies of fast electrons in the edge plasma within the tokamak--type devices of different operational parameters. It is possible to customize such detectors for specific tokamaks, but one must take into account the expected experimental conditions in order to modify the Cherenkov probe in an appropriate way.
- Particular attention should be paid to the possibility of identification of the fast-electron generation regions and the registration of fast-electron burst precursors, which might be used for controlling long-lasting tokamak discharges.

Acknowledgment. The studies reported in this paper were carried out within the P3 task of the research programme supported by the EURATOM Community under the contract with the Association EURATOM-IPPLM, Poland (contract no. FU06-CT-2004-00081); they were also supported by the Ministry of Higher Education and Science, Poland, under the contract no. 47/EURATOM/2005/7. The views and opinions expressed herein do not necessarily reflect those of the European Commission.

References

1. Barnes CW (1981) Studies of runaway electron transport in PLT and PDX. PhD thesis, Princeton University, USA
2. Basiuk V, Bergeaud V, Chantant M *et al*. (2000) Ripple loss studies during ICRF heating on Tore Supra. In: Proc of the 27th EPS Conf on Controlled Fusion and Plasma Physics, 12–16 June 2000, Budapest, Hungary. ECA 24B:784–787
3. Basiuk V, Eriksson L-G, Bergeaud V *et al*. (2004) Ripple losses during ICRF heating in Tore Supra. Nucl Fusion 44:181–192
4. Hoenen F, Graffmann E, Finken KH *et al*. (1994) Liquid scintillation detectors for gamma and neutron diagnostics at TEXTOR and results of runaway and sawtooth oscillations. Rev Sci Instrum 65:2594–2598
5. Jakubowski L, Malinowski K, Sadowski MJ *et al*. (2010) Study of electron beams within ISTTOK tokamak by means of a multi-channel Cherenkov detector; their correlation with hard X-rays. Nucl Instrum Methods Phys Res A 623:686–689
6. Jakubowski L, Rabinski M, Stanislawski J, Sadowski MJ, Zebrowski J (2006) Feasibility study and design of Cherenkov-type detectors for measurements of fast electrons within tokamaks. Probl Atom Sci Tech 1, Series Plasma Phys 13:206–208
7. Jakubowski L, Sadowski MJ (2005) Measurements of pulsed electron beams emitted from plasma-focus devices. Probl Atom Sci Techn 1, Series Plasma Phys 10:89–91
8. Jakubowski L, Sadowski MJ, Stanisławski J *et al*. (2007) Application of Cherenkov detectors for fast electron measurements in CASTOR tokamak. In: Proc of the 34th EPS Conf on Controlled Fusion and Plasma Physics, 2–6 July 2007, Warsaw, Poland. ECA 31F:5.097
9. Jakubowski L, Sadowski M, Zebrowski J (1997) Investigation of new Cherenkov-type detectors for studies of fast electron beams emitted from hot plasma. J Techn Phys 38:141–150
10. Jakubowski L, Sadowski MJ, Zebrowski J *et al*. (2010) Cherenkov-type diamond detectors for measurements of fast electrons in the TORE-SUPRA tokamak. Rev Sci Instrum 81:013504
11. Jakubowski L, Stanislawski J, Sadowski MJ, Zebrowski J, Weinzettl V, Stockel J (2006) Design and tests of Cherenkov detector for measurements of fast electrons within CASTOR tokamak. Czech J Phys 56:B98–B103
12. Jaspers R, Finken KH, Mank G *et al*. (1992) Observation of relativistic runaway electrons by synchrotron radiation in TEXTOR. In: Proc of the Int Conf on Plasma Physics, 29 June – 3 July 1992, Innsbruck, Austria. Part I:155
13. Jaspers R, Lopez Cardozo NJ, Finken KH (1993) Confinement of relativistic electrons in TEXTOR. In: Proc of the Workshop on Local Transport Studies in Fusion Plasmas, 12–16 July 1993, Varenna, Italy. Part I:193
14. Kawashima H, Sato M, Tsuzuki K *et al*. (2001) Demonstration of ripple reduction by ferritic steel board insertion in JFT-2M. Nucl Fusion 41:257–263
15. Knoepfel H, Spong DA (1979) Runaway electrons in toroidal discharges. Nucl Fusion 19:785–829
16. Kruskal M, Bernstein IB (1964) Runaway electrons in an ideal Lorentz plasma. Phys Fluids 7:407–418
17. Kulsrud RM, Sun YC, Winsor NK, Fallon HA (1973) Runaway electrons in a plasma. Phys Rev Lett 31:690–693
18. Laurent L, Rax JM (1990) Stochastic instability of runaway electrons in tokamaks. Europhys Lett 11:219–224
19. Lipa M, Martin G, Mitteau R *et al*. (2003) Effects of suprathermal particle impacts on TORE SUPRA plasma facing components. Fusion Engin Design 66/68:365–369
20. Martin G (1998) Runaway electrons: from TORE--SUPRA to ITER. In: Proc of the 25th EPS Conf on Controlled Fusion and Plasma Physics, 29 June – 3 July 1998, Prague, Czech Republic. ECA 22C:651–654
21. Mitteau R, Chappuis Ph, Martin G *et al*. (2001) Analysis of an in-service rupture of the inner first wall of TORE SUPRA. Fusion Engin Design 56/57:445–449
22. Plyusnin VV, Cabral JAC, Figueiredo H, Nezelskii IS, Varandas CAF (2002) Self-consistent analysis of the power-energy balance and determination of the run-

away electron characteristics in the ISTTOK discharges. Plasma Phys Control Fusion 44:2021–2031
23. Plyusnin VV, Jakubowski L, Zebrowski J *et al*. (2008) Use of Cherenkov-type detectors for measurements of runaway electrons in the ISTTOK tokamak. Rev Sci Instrum 79:10F505
24. Rechester AB, Rosenbluth MN (1978) Electron heat transport in a tokamak with destroyed magnetic surfaces. Phys Rev Lett 40:38–41
25. Sadowski MJ, Jakubowski L, Szydlowski A (2004) Adaptation of selected diagnostic techniques to magnetic confinement fusion experiments. Czech J Phys 54:C74–C81
26. Yushmanov PN (1987) Diffuse transport process caused by ripple in tokamak. In: Kadomtsev BB (ed) Reviews of plasma physics. Vol. 16. Consultants Bureau, New York, p 117
27. Zebrowski J, Jakubowski L, Sadowski MJ *et al*. (2007) Diagnostics of fast electrons within CASTOR tokamak by means of a modified Cherenkov-type probe. In: Proc of the Int Conf PLASMA-2007, 16–19 October 2007, Greifswald, Germany. AIP CP 993:255–258
28. Zehrfeld HP, Fussman G, Green BJ (1981) Electric field effects on relativistic charged particle motion in tokamaks. Plasma Phys 23:473–489
29. Zrelov VP (1970) Cherenkov radiation in high energy physics. Part I. Atomizdat, Moscow (Translation: Israel Program for Scientific Translations, Jerusalem)